

Vortex Solitons and Filamentation of Electromagnetic Beams in Relativistically Degenerate Plasmas

N. Maltsev¹ and V.I. Berezhiani^{1,2}

¹*School of Physics, Free university of Tbilisi, Tbilisi 0159, Georgia and*

²*Andronikashvili Institute of Physics (TSU), Tbilisi 0177, Georgia.*

We study the propagation and stability of electromagnetic vortex beams in relativistically degenerate plasmas. We show that such plasmas support localized vortex solitons carrying orbital angular momentum and analyze their linear and nonlinear stability. Vortex solitons undergo azimuthal symmetry-breaking instabilities whose growth rates depend on beam power, propagation constant, and topological charge, with the dominant mode determining the number of filaments formed during breakup. We further demonstrate that vortex solitons act as nonlinear attractors with a finite basin of attraction, while the vortex core remains topologically protected, maintaining a strictly zero field intensity at the beam center throughout the evolution. The results persist across a broad range of degeneracy parameters and are relevant to hard X -ray radiation propagating in dense astrophysical plasmas.

I. INTRODUCTION

Astrophysical systems are characterized by intense electromagnetic radiation whose spectral content spans a broad range, from radio waves to hard X -ray and γ -ray emission [1]. Most cosmic objects - such as stars, interstellar and intergalactic media, active galactic nuclei, and quasars - are either composed of plasma or embedded in a plasma environment [2]. In many of these systems, radiation propagates through regions of extremely high density, where collective plasma effects play a dominant role in shaping wave dynamics. For the ultrahigh plasma densities relevant to compact astrophysical objects, including the interiors of white dwarfs, neutron stars, pre-supernova cores, and possibly the central engines of gamma-ray bursts [3], the classical plasma description becomes inadequate. Under such conditions, the electron gas is degenerate and must be described using Fermi-Dirac statistics. The corresponding Fermi energy exceeds the atomic binding energy, leading to complete ionization of matter. Typical electron number densities in these environments are believed to lie in the range from 10^{26} cm^{-3} to 10^{34} cm^{-3} , where the average interparticle spacing becomes smaller than the thermal de Broglie wavelength and the plasma behaves as a weakly coupled degenerate system [4]. At the same time, compact astrophysical systems are known to host extremely intense high-frequency radiation fields. In particular, strong and spectrally narrow X -ray emission may arise from cyclotron harmonics in strongly magnetized environments [5], atomic line emission from highly ionized species in accretion-powered sources [7], or external irradiation by localized compact objects such as neutron stars and white dwarfs [6]. In many situations of interest, dense plasma layers remain transparent to X -ray radiation due to the suppression of collisional absorption at high frequencies and the dominance of electron degeneracy effects, allowing electromagnetic waves to propagate over macroscopic distances.

A series of studies has examined nonlinear interactions between high-frequency electromagnetic (EM) radiation and plasma waves in degenerate media. Stimulated scattering processes were analyzed in Refs. [8]-[10], demonstrating the emergence of instabilities in both weakly and strongly degenerate electron plasmas. Refs. [11]-[13] investigated solitary solutions in fully degenerate relativistic and nonrelativistic multi-species plasmas, showing that such nonlinear structures are stable against small perturbations and persist across the full range of degeneracy levels.

The self-trapped propagation of EM beams in fully degenerate relativistic electron-positron and electron plasmas has been investigated in (1+2)-dimensional geometries [14],[15] demonstrating the existence of radially symmetric, localized EM structures supported by self-guiding mechanisms in these plasmas.

Electromagnetic beams carrying orbital angular momentum, known as vortex beams, possess a phase singularity and an annular intensity profile. Under laboratory conditions, vortex beams can be produced using phase plates, holographic techniques, or mode-conversion schemes (see Ref. [16] and references therein). In astrophysical settings, twisted EM fields may arise naturally due to rotation of compact objects, frame-dragging effects, or propagation through inhomogeneous media, imprinting angular momentum onto radiation [17],[18].

Recent work [19] examined the nonlinear propagation of orbital-angular-momentum-carrying electromagnetic beams in highly degenerate relativistic electron-positron plasmas. Because the high-frequency electromagnetic pressure acts equally on electrons and positrons, charge separation is suppressed, and, within the paraxial approximation, the beam dynamics is governed by a nonlinear Schrödinger equation with saturating nonlinearity.

In the present work, we base our analysis on the system of nonlinear equations describing electromagnetic beam propagation in degenerate electron plasmas, derived in previous studies [10],[15]. We extend this framework to investigate the propagation of vortex electromagnetic beams. Unlike in the electron–positron plasma case, the system cannot be reduced to a single nonlinear Schrödinger equation; instead, one must analyze a coupled set of nonlinear equations. The presence of orbital angular momentum qualitatively modifies the nonlinear interaction. We demonstrate that degenerate electron plasmas can support localized vortex-type electromagnetic structures whose properties differ from those of non-vortex beams, thereby highlighting the role of beam topology in relativistic plasma dynamics.

II. MODEL

As shown in Ref. [10], the dynamics of relativistic electromagnetic beams propagating in a degenerate electron plasma can be described by a set of nonlinear equations which, in dimensionless form, read as follows.

$$2i\frac{\partial A}{\partial z} + \nabla_{\perp}^2 A + \left(1 - \frac{N}{1 + \Psi}\right) A = 0 \quad (1)$$

$$\nabla_{\perp}^2 \Psi + 1 - N = 0 \quad (2)$$

$$N = \frac{(1 + \Psi) \left[(1 + \Psi)^2 - (1 + |A|^2 - d) \right]^{3/2}}{d^{3/2} \left[(1 + \Psi)^2 - |A|^2 \right]^{1/2}} \quad (3)$$

Here A is the slowly varying amplitude of circularly polarized vector potential $e\mathbf{A}/(m_e c^2 \Gamma_0) = (\hat{\mathbf{x}} + i\hat{\mathbf{y}}) A \exp(-i\omega_0 t - k_0 z) + c.c.$, where $\hat{\mathbf{x}}$ and $\hat{\mathbf{y}}$ are unite vectors transverse to the electromagnetic beam propagation direction z . The field frequency ω_0 and wave vector k_0 satisfy the dispersion relation $\omega_0^2 = k_0^2 c^2 + \omega_e^2 / \Gamma_0$, with $\omega_e = (4\pi e^2 n_0 / m_e)^{1/2}$ being the plasma frequency, n_0 the equilibrium electron density, and $\Gamma_0 = (1 + R_0^2)^{1/2}$ the generalized relativistic factor, where $R_0 = (n_0 / n_c)^{1/3}$ with $n_c = m_e^3 c^3 / 3\pi^2 \hbar^3 = 5.9 \times 10^{29} \text{ cm}^{-3}$. The normalized potential is defined as $\Psi = e\varphi / (m_e c^2 \Gamma_0)$ where φ is the charge-separation scalar potential generated by the action of the high-frequency electromagnetic pressure on electrons. The normalized electron density is $N = N/n_0$. The dimensionless spatial variables are introduced as $z = (\omega_e^2 / c\omega_0 \Gamma_0) z$, and $\mathbf{r}_{\perp} = (\omega_e / c\sqrt{\Gamma_0}) \mathbf{r}_{\perp}$. In Eq. (3) the parameter $d = R_0^2 / (1 + R_0^2)$ quantifies the level of degeneracy: for the weakly degenerate case ($R_0 \ll 1$) $d \simeq R_0^2$, whereas in the relativistically degenerate regime ($R_0 \gg 1$) $d \rightarrow 1$.

Deriving the system of Eqs. (1)–(3) it is assumed that plasma is highly transparent $\omega_e / \omega_0 \ll 1$ and $\lambda \ll L_{\perp} \ll L_{\parallel}$ where $\lambda \approx 2\pi c / \omega_0$ is the wavelength of EM radiation, L_{\perp} and L_{\parallel} are the characteristic longitudinal and transverse spatial dimensions of the EM beam. This system describes the dynamics of strong amplitude narrow EM beams in plasma with arbitrary (but physically justified) strength of degeneracy. The gas approximation for degeneracy plasma implies that particle interaction should be less the Fermi energy. This condition implies that plasma electron density should be $n_0 \geq e^6 m_e^3 / \hbar^6 = 6.7 \times 10^{24} \text{ cm}^{-3}$ and consequently $R_0 \gg 0.02$, note that for $n_0 = n_c = 5.9 \times 10^{29} \text{ cm}^{-3}$, $R_0 = 1$ while $n_0 = 10^{34} \text{ cm}^{-3}$ corresponded to the ultra-relativistic degeneracy with $R_0 \approx 26$. For the electron densities $10^{26} \text{ cm}^{-3} - 10^{34} \text{ cm}^{-3}$ the level of degeneracy measure d in Eq.(3) varies in the range $0.003 < d < 0.999$.

For strongly relativistic degenerate plasma ($d \rightarrow 1$) we get the following set of equations

$$2i\frac{\partial A}{\partial z} + \nabla_{\perp}^2 A + \left(1 + |A|^2 - (1 + \Psi)^2\right) A = 0 \quad (4)$$

$$\nabla_{\perp}^2 \Psi + 1 + (1 + \Psi) \left(|A|^2 - (1 + \Psi)^2 \right) = 0 \quad (5)$$

Let us now consider the solitary wave solutions carrying vortices. Assuming that solutions in polar coordinates are of the form $A = \hat{A}(r) \exp(im\theta + ikz/2)$ and $\Psi = \hat{\Psi}(r)$ where $r = \sqrt{x^2 + y^2}$ and θ is the polar angle, Eqs. (4) and (5) reduce to ordinary differential equations for the real valued amplitude \hat{A} and potential $\hat{\Psi}$ as follows:

$$\frac{d^2\hat{A}}{dr^2} + \frac{1}{r} \frac{d\hat{A}}{dr} - k\hat{A} - \frac{m^2}{r^2}\hat{A} + \left(1 + \hat{A}^2 - (1 + \hat{\Psi})^2\right)\hat{A} = 0 \quad (6)$$

$$\frac{d^2\hat{\Psi}}{dr^2} + \frac{1}{r} \frac{d\hat{\Psi}}{dr} + 1 + (1 + \hat{\Psi}) \left(\hat{A}^2 - (1 + \hat{\Psi})^2\right) = 0 \quad (7)$$

Here k is a propagation constant and $m(\neq 0)$ is an integer known as the topological charge of the vortex.

We have used numerical methods to determine localized solutions of Eqs. (6)–(7) subject to the boundary conditions $(\hat{A}, \hat{\Psi}) \rightarrow 0$ as $r \rightarrow \infty$, while $\hat{A}_{r \rightarrow 0} \rightarrow A_0 r^{|m|}$, $\hat{\Psi}_{r \rightarrow 0} \rightarrow \Psi_0$, $(d\Psi/dr)_{r \rightarrow 0} \rightarrow 0$. In what follows, we consider only the lowest-order (lowest radial eigenmode) solutions of Eqs. (6) and (7). Such solutions imply that the vector potential has a node at the origin $r = 0$ reaches a maximum at a finite radius, and then monotonically decreases with increasing r , whereas the scalar potential is nodeless, also reaches a maximum, and decays with increasing r . To obtain such solutions for a given propagation constant $k > 0$, one must determine the appropriate values of the constants A_0 and Ψ_0 with high accuracy. This is achieved numerically by solving Eqs. (6)–(7) as a boundary-value problem, employing a shooting method in which the parameters A_0 and Ψ_0 are iteratively adjusted to satisfy the localization conditions at large radii. For $m = 1$ and $k = 0.2$, localized solitary solutions are found for $A_0 = 0.368$ and $\Psi_0 = 0.065$. The corresponding radial profiles of the electromagnetic fields and the electron density are shown in Fig. 1(a). Similar field structures are obtained for other values of the propagation constant provided that $k < 1$. In Fig. 1(b), we present the field and density profiles for $k = 0.3$. It is evident that, with increasing k , the amplitudes of the field components \hat{A}_m and $\hat{\Psi}_m$ increase. As shown in Fig. 2, these amplitudes are monotonically increasing functions of k . We emphasize that, simultaneously, the electron density becomes increasingly depleted as the potentials reach their maximal values at r_m , and in the limit $k \rightarrow k_c = 0.3$ the density tends to zero, indicating the onset of electron cavitation. Note, however, that for $k > k_c$ the electron density becomes negative, and therefore the plasma model based on a fluid description is no longer applicable.

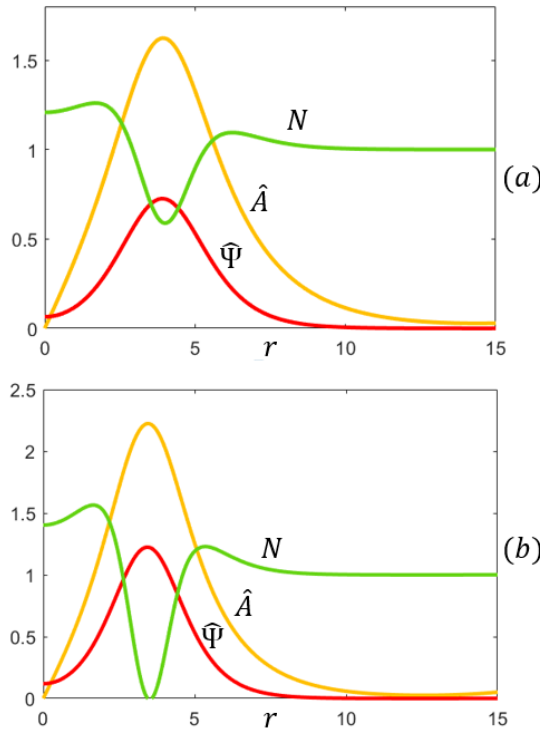


FIG. 1: Numerically found stationary potential profiles for $m = 1$, $k = 0.2$ (a) and $k = 0.3$ (b)

A similar qualitative behavior is observed for vortex solutions with higher topological charge. In particular, for $m = 2$, localized solutions also exist provided that the propagation constant satisfies the same condition as in the

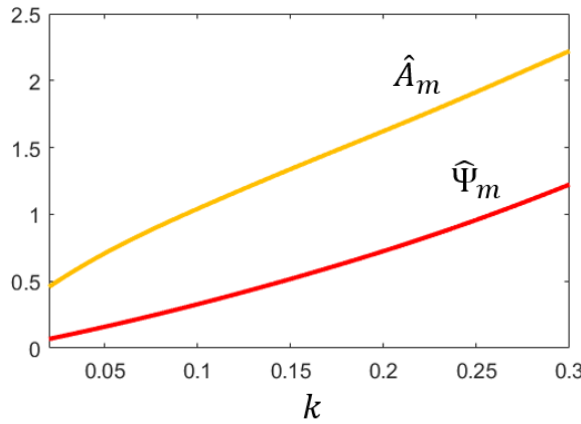


FIG. 2: Stationary $m = 1$ vortex amplitudes as functions of k

$m = 1$ case. Within this domain, higher-charge vortices exhibit the same generic features as the fundamental vortex, including annular field localization and electron density depletion leading to cavitation as $k \rightarrow k_c$. Not only does changing the topological charge preserve the existance domain, but it also causes negligible changes to the cavitation condition and the amplitude dependence on the propogation constant. As shown of Fig. 3, the vortex solution for $k = 0.2$ and $m = 2$ is just a wider version of its lower topological charge predecessor.

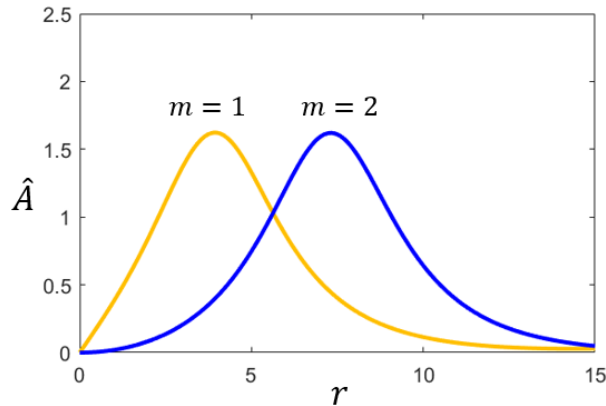


FIG. 3: Numerically found stationary potential profiles for $k = 0.2$, $m = 1$ and $m = 2$

The EM beam power $P = \int d\mathbf{r}_\perp |A|^2$ is an integral of motion of the system of Eqs. (1)–(3). For an EM field carrying a nonzero topological charge, the system admits an additional conserved quantity, namely the angular momentum,

$$L = \frac{i}{2} \int d\mathbf{r}_\perp \left[x \left(A^* \frac{\partial A}{\partial y} - c.c. \right) - y \left(A^* \frac{\partial A}{\partial x} - c.c. \right) \right] \quad (8)$$

This expression represents the paraxial approximation to the orbital angular momentum of the EM field. One can readily show that, for steady-state solutions, the angular momentum is fully determined by the topological charge and the beam power, yielding the relation $L = mP$.

As follows from numerical simulations of Eqs. (6) and (7), the power trapped in self-guided vortex solitons,

$$P = 2\pi \int_0^\infty dr r \hat{A}^2 \quad (9)$$

is a monotonically increasing function of the propagation constant k ($dP/dk > 0$). Since k is itself an increasing function of \hat{A}_m , it is convenient to present the dependence of the trapped power on \hat{A}_m , as shown in Fig. 4. One can

see that, in the strongly degenerate case, the power trapped in a singly charged ($m = 1$) vortex solitonic structure is bounded from below by a finite value $P_0 = 145$, which is reached at small amplitudes $\hat{A}_m \ll 1$ (i.e., in the limit $k \rightarrow k_c$). The upper bound of the trapped power, $P_c = 283$, is associated with electron cavitation occurring at larger amplitudes $\hat{A}_{mc} = 2.221$ (corresponding to $k \rightarrow k_c$).

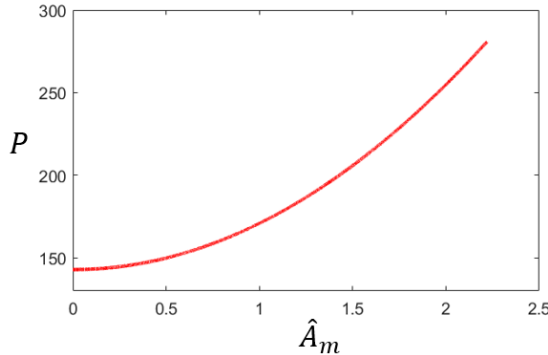


FIG. 4: Power carried by the stationary state as a function of its amplitude

We now turn to the stability analysis of vortex solitons. Numerous analytical and numerical studies have shown that ring-shaped vortex beams described by nonlinear Schrödinger equations with saturating nonlinearity in various media are susceptible to azimuthal symmetry-breaking modulational instability [20], [21]. Although the present system differs from the standard nonlinear Schrödinger equation due to the coupling between the electromagnetic field and the plasma response, the qualitative features responsible for the azimuthal instability remain similar. In particular, the self-focusing nonlinearity combined with the ring-shaped intensity distribution of vortex solitons creates favorable conditions for azimuthal modulation growth. We therefore expect that vortex solitons supported by degenerate relativistic electron plasmas will exhibit a qualitatively similar instability scenario. The stability of vortex solitons can be analyzed by following the linear stability procedure developed in [22] (see also [23]). In this approach, one considers small perturbations acting along a ring of mean radius r_m where $\hat{A}(r_m) = \hat{A}_m$ and $\hat{\Psi}(r_m) = \hat{\Psi}_m$. Assuming constant intensities and spatial uniformity for this ring, one can rewrite the operator in (6) and (7) as $\nabla_\perp^2 = r_m^{-2} \partial^2 / \partial \theta^2$. The growth rate of azimuthal perturbations with phase factor $\phi = Kz + M\theta$, where M is an integer azimuthal mode number, can then be derived in the form

$$\text{Im}(K) = \frac{1}{2} \frac{M}{r_m} \left[2\hat{A}_m^2 - \frac{M^2}{r_m^2} - Q \right]^{1/2}. \quad (10)$$

Where

$$Q = 4\hat{A}_m^2 \left(1 + \hat{\Psi}_m \right)^2 \left(\frac{M^2}{r_m^2} + \frac{1}{1 + \hat{\Psi}_m} + 2 \left(1 + \hat{\Psi}_m \right)^2 \right)^{-1} \quad (11)$$

The function under the root is positive for some integer values of M in the studied range of propagation constant k , implying the existence of azimuthal instabilities. In Fig. 5 we plot $\text{Im}(K)$ versus M for different values of k . The parameters r_m , \hat{A}_m and $\hat{\Psi}_m$ are all calculated via the localized solutions of equations (6) and (7). The integer value of M for which $\text{Im}(K)$ is maximal gives the approximate number of modulations that affect the ring.

To verify the predictions of the linear stability analysis, we numerically solved the system of Eqs. (4) and (5) using finite-difference methods. As initial conditions, we employed the stationary solutions of Eqs. (6)–(7) obtained for different values of the propagation constant $k < k_c$. Since any finite-difference discretization approximates partial differential equations with limited accuracy, the use of stationary solutions as initial conditions introduces an inherent small perturbation. Our numerical simulations show that this perturbation rapidly triggers an instability, in agreement with the predictions of the linear stability analysis.

In Fig. 6, we present the results of a representative simulation in which the initial condition corresponds to $k = 0.2$. We split each discrete step into linear and non-linear parts, respectively using Crank-Nicolson and Euler methods for their solution. One observes that the instability leads to the breakup of the vortex soliton into four filaments, in accordance with the dominant azimuthal mode predicted by the linear stability analysis. The breakup occurs at $z_{br} \approx 70$ while the corresponding diffraction length is $z_D \approx 20$. This implies that the vortex solitary wave decays

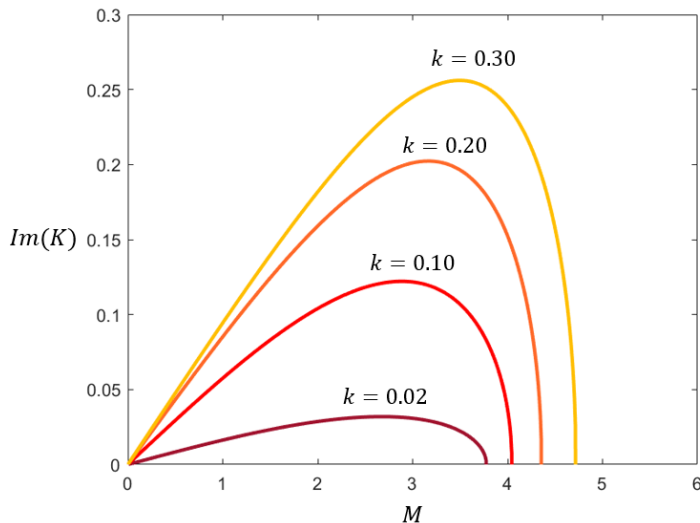


FIG. 5: $\text{Im}(K)$ as a function of M for $k = 0.02, 0.10, 0.20$ and 0.3

after propagating over 3.5 diffraction lengths. As shown in Fig. 7 the filaments propagate tangentially away from the original ring-shaped intensity distribution, conserving the total angular momentum L of the electromagnetic field. As they separate, the filaments evolve into stable, spatially localized solitonic beams carrying zero topological charge. Similar behavior is observed for vortex solitons with higher values of m .

The next question to investigate concerns the nonlinear stability of electromagnetic fields carrying topological charge under non-ideal excitation conditions, when the initial spatial profile and field strength differ substantially from those of the stationary vortex soliton solution. This analysis is particularly relevant for realistic beam generation, where exact soliton profiles cannot be prepared. For this purpose, we consider a Gaussian input beam of the form

$$A(z = 0, x, y) = (x + iy) A_1 \exp(-r^2/D^2) \quad (12)$$

which carries a topological charge $m = 1$. The beam intensity vanishes at $r = 0$, reaches its maximum value $A_{\max} = A_1 D \exp(-0.5)$ at $r_{\max} = D$, and decays exponentially for larger r . Here D is the characteristic transverse width of the structure, and A_1 is a constant which, together with D , determines the electromagnetic beam power $P = \frac{\pi}{4} A_1^2 D^4$.

We numerically integrate Eqs. (4)–(5), assuming $P < P_c$. For powers below a threshold value $P < P_0 \approx 145$, the beam undergoes diffraction. In contrast, for intermediate powers $P_0 < P < P_c$, the evolution is governed by nonlinear self-organization and instability. When the initial beam parameters lie within the basin of attraction of the stationary vortex soliton, and the initial amplitude is chosen close to the soliton value $A_{\max} \approx \hat{A}_m$, the Gaussian vortex exhibits partial relaxation toward the ground-state vortex soliton through radiation losses. This quasi-relaxed state remains azimuthally unstable and subsequently breaks up into multiple filaments. The filaments are expelled tangentially with respect to the initial ring-shaped intensity distribution and evolve into stable, spatially localized solitonic beams just as it occurred for stationary initial conditions. If the initial Gaussian beam parameters (P, A_m) lie far outside the basin of attraction of the vortex soliton, the structure does not approach the soliton configuration. Nevertheless, the qualitative evolution remains similar, with filamentation occurring at earlier propagation distances.

Similar behavior is observed for vortex beams with higher topological charge. It should be noted, however, that high-charge vortices are generally believed to be unstable even during vacuum propagation due to topological considerations, which imply that such beams tend to decay into multiple single-charge vortices. This decay, however, is governed by an algebraic (secular) instability, whereas the breakup observed in our system is exponential. Consequently, the secular instability does not have sufficient time to develop before the onset of the nonlinear azimuthal instability. We emphasize that optical vortices possess a topological nature, corresponding to branch points where both the real and imaginary parts of the field vanish simultaneously. The topological charge is defined by the number of intersecting pairs of zero lines of the real and imaginary components of the field. As a result, a vortex embedded in an electromagnetic beam cannot disappear under continuous deformations of the field, even when the beam undergoes substantial structural changes. An important and experimentally attractive feature of the breakup process described above is that, despite the fragmentation of the beam, the field amplitude at the center of the structure remains strictly

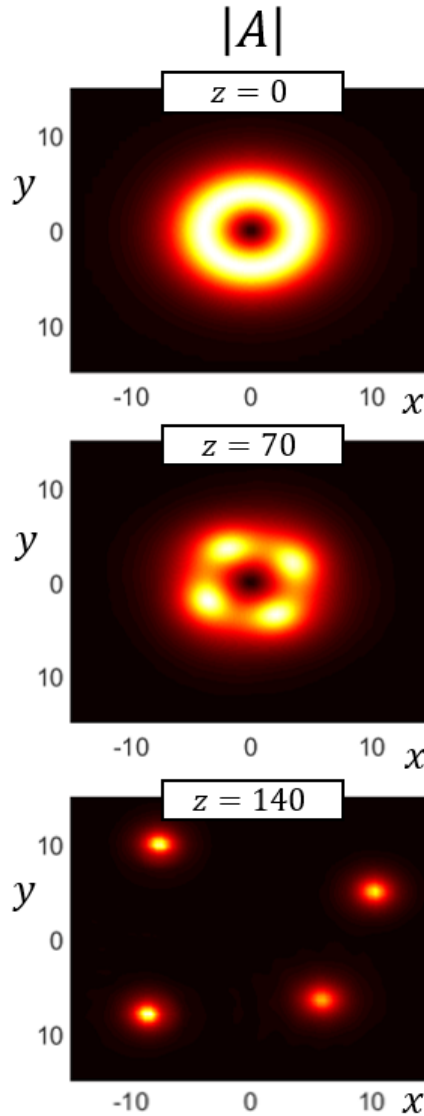


FIG. 6: Numerically achieved evolution of $k = 0.2$, $m = 1$ vortex soliton

zero throughout the evolution. This topological robustness provides a clear and unambiguous signature that can be exploited for experimental verification.

Although throughout most of this manuscript we have focused on the ultrarelativistic degeneracy regime ($d = 1$) we have also performed analogous studies for other values of the degeneracy parameter, namely $d = 0.5$ and $d = 0.01$ corresponding to plasma densities $n_0 = 5.96 \times 10^{29} \text{ cm}^{-3}$ and $n_0 = 5.96 \times 10^{26} \text{ cm}^{-3}$, respectively. In all cases, the underlying physics and the qualitative features of the beam dynamics remain essentially the same as those obtained for $d = 1$. Both the threshold power P_0 and the admissible field amplitudes decrease with decreasing d . For example, we find $P_0 \approx 120$ for $d = 0.5$ and $P_0 = 95$ for $d = 0.01$.

Restoring the dimensions, the corresponding threshold power can be written as

$$P_0^{(\text{dim})} \simeq 0.17 \left(\frac{\omega_0}{\omega_e} \right)^2 \Gamma_0 R_0^2 P_0 \text{ GW}, \quad (13)$$

where $P_0^{(\text{dim})}$ is measured in GW. For degeneracy parameter in the range $d = 0.01 - 0.5$, required beam power lies in the interval $P_0^{(\text{dim})} = (15.6 - 20.5) \text{ GW}$. Since plasma is assumed to be transparent, the photon energy of the beam must satisfy $\hbar\omega_0 \gg (1 \text{ keV} - 29 \text{ keV})$, placing the relevant frequency range in the hard X-ray band.

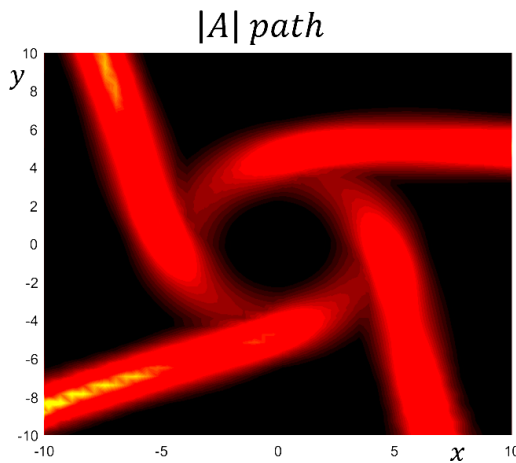


FIG. 7: The soliton trajectories for the $k = 0.2, m = 1$ vortex

III. CONCLUSIONS

We have studied the propagation and stability of electromagnetic vortex beams in relativistically degenerate plasmas using a self-consistent relativistic fluid–Maxwell model. We demonstrated the existence of localized vortex solitons carrying orbital angular momentum and analyzed their linear and nonlinear stability.

Vortex solitons are shown to undergo azimuthal symmetry-breaking instabilities whose growth rates depend on the beam power, propagation constant, and topological charge. The dominant unstable mode determines the number of filaments formed during breakup, in agreement with linear stability theory. Although multiply charged vortices are known to exhibit slow, algebraic splitting even in vacuum, the instability identified here is exponential and develops on much shorter scales, making secular decay irrelevant in dense plasmas.

We further examined the nonlinear evolution of non-ideal Gaussian vortex beams and found that vortex solitons act as nonlinear attractors with a finite basin of attraction. Depending on the initial parameters, beams either diffract or undergo partial relaxation toward the stationary vortex soliton followed by filamentation. Throughout the evolution, the vortex core remains topologically protected, with the field intensity at the beam center remaining strictly zero.

These results persist across a broad range of degeneracy parameters, although the admissible power range decreases with decreasing degeneracy. Estimates of the dimensional threshold power place the relevant regime in the hard X-ray band and at multi-gigawatt beam powers, conditions naturally realized in dense astrophysical environments near compact objects.

The research was supported by the Shota Rustaveli National Science Foundation grant No. FR-24-1751. The research of N.M. was supported by the Knowledge Foundation at the Free University of Tbilisi.

[1] M. C. Begelman, R. D. Blandford, and M. D. Rees, *Rev. Mod. Phys.* **56**, 255 (1984).
[2] V.V.Zheleznyakov, *Radiation in astrophysical plasmas* (Kluwer Academic Publishers, 1996).
[3] S.L. Shapiro and S.A. Teukolsky, *Black Holes, White Dwarfs, and Neutron Stars: The Physics of Compact Objects* (Wiley-VCH, Weinheim, 2004).
[4] L.D. Landau and E.M. Lifshitz, *Statistical Physics* (Pergamon Press, 1980).
[5] A.K. Harding and D. Lai, *Rep. Prog. Phys.* **69**, 2631 (2006).
[6] W. H. G. Lewin, J. van Paradijs, and E. P. J. van den Heuvel, *X-Ray Binaries* (Cambridge University Press, Cambridge, 1995).
[7] A.C. Fabian, K. Iwasawa, C.S. Reynolds, and A.J. Young, *PASP*, **112**, 1145 (2000).
[8] G. T. Chanturia, V. I. Berezhiani, and S. M. Mahajan, *Phys. Plasmas* **24**, 074501 (2017).
[9] A. P. Misra and D. Chatterjee, *Phys. Plasmas* **25**, 062116 (2018).
[10] R. M. Goshadze, V. I. Berezhiani, and Z. Osmanov, *Phys. Lett. A* **383**, 1027 (2019).
[11] V. I. Berezhiani, N. L. Shatashvili, and N. L. Tsintsadze, *Phys. Scripta* **90**, 068005 (2015).
[12] G. Mikaberidze, and V.I. Berezhiani, *Phys. Lett. A* **379**, 2730 (2015).
[13] N. L. Shatashvili, S. M. Mahajan, and V. I. Berezhiani, *Phys. Plasmas* **27**, 012903 (2020).

- [14] V.I. Berezhiani and N.L. Shatashvili, *Phys. Plasmas* **23**, 104502 (2016).
- [15] V.I. Berezhiani, Z.N. Osmanov, S.M. Mahajan, S.V. Mikeladze, *Phys. Plasmas* **28**, 052104 (2021).
- [16] Y. Shen, X. Wang, Z. Xie, C. Min, X. Fu, Q. Liu, M. Gong, and X. Yuan, *Light Sci. Appl.* **8**, 90 (2019).
- [17] M. Harwit, *Astrophys. J.* **579** 1266 (2003).
- [18] F. Tamburini, B. Thide, M. Valle, *Mon. Not. R. Astron. Soc.* **492**, 22 (2020).
- [19] V.I. Berezhiani, Z.N. Osmanov, and S.V. Mikeladze, *Phys. Lett. A* **448**, 128323 (2022).
- [20] W. J. Firth and D. V. Skryabin, *Phys. Rev. Lett.* **79**, 2450 (1997).
- [21] A. S. Desyatnikov, Y. S. Kivshar, and L. Torner, *Prog. Opt.* **47**, 2910 (2005).
- [22] J. Atai, Y. Chen, and J.M. Soto-Crespo, *Phys. Rev. A* **49**, 3170 (1994).
- [23] A. Vincotte and L. Berge, *Physica D* **223**, 163 (2006).